Hypersonic Ludwieg Tube

Rolf Radespiel, Malte Estorf, Dirk Heitmann, Federico Muñoz and Torsten Wolf

1 Introduction

The aerothermal design of vehicles operating at hypersonic speeds calls for a good knowledge of aerodynamic and thermal loads on the vehicle components. While significant progress has been achieved in the development of accurate and efficient numerical flow simulation methods there still exist a number of hypersonic flow phenomena where flow experiments are needed to achieve acceptable uncertainty levels in vehicle design. Among these are laminar-turbulent transition of boundary layers and shock-boundary layer interactions. Hypersonic flow research over several decades has resulted in significant theories and a large amount of measured data on these subjects. Nevertheless, the flow physics is extremely complex, and numerical flow simulations cannot resolve the complete range of temporal and spatial flow scales involved. Hence there is the need for fundamental flow experiments in these fields.

Hypersonic flight usually takes place at high flow velocities and high flow enthalpies. This makes representative flow experiments in wind tunnels very difficult as the high enthalpies introduce extreme heat loads on the facility and on the investigated wind tunnel models, not to speak of the extreme kinetic energy rate needed to establish a high-enthalpy hypersonic air stream. Hence, realistic flight enthalpy levels can only be simulated in a few, expensive facilities worldwide and only during a few milliseconds of intermittent runtime. The experimentation opportunities offered by these facilities are therefore too limited in fulfilling the

---

Contribution to "Experimental Methods of Shock Wave Research".

R. Radespiel (✉) · M. Estorf · D. Heitmann · F. Muñoz · T. Wolf
Technische Universität Braunschweig, 38106 Braunschweig, Germany
e-mail: r.radespiel@tu-bs.de

needs of research institutions interested in the fundamentals of hypersonic flow physics. This is why many fundamental problems in hypersonics are investigated in flow facilities where the Mach and Reynolds numbers are properly simulated but at lower than in a real flight flow enthalpy.

The typical research institutes involved in these fundamental research works can only afford a limited investment into a facility and relatively low operation cost. Typical values for these cost constraints are one Million US dollars for the facility and a few US dollars for the consumables needed per run. In addition, a suitable facility should be operated by the flow researcher alone, without assistance of a specially trained technician.

Top-level requirements for a hypersonic research facility call for a Mach number high enough that typical hypersonic flow behaviors are achieved for blunt and slender configurations. Furthermore, in order to enable testing of laminar and turbulent flows, the facility should provide a Reynolds-number of 15×10^6, based on the model length. The test time should be in the order of 100 ms in order to allow for a range of useful flow measurement techniques.

Continuous progress in wind tunnel engineering and in instrumentation available for flow measurements in hypersonics over the last decades has resulted in a specific wind tunnel configuration that meets these requirements. This is the hypersonic Ludwieg tube. Several of these gas dynamics facilities are in operation worldwide. The present contribution describes one of the successful designs of this kind, along with data that characterize the quality and capabilities of this facility.

2 Ludwieg Tube Design

The working principle of the Ludwieg tube goes back to the 1950s [1]. Hubert Ludwieg analyzed the cost effectiveness of high-speed wind tunnels, then in operation. He pointed out that the relative cost advantage of the blow-down wind tunnel relative to the in draft tunnel increases with tunnel Mach number. If the needed run time for testing is only in the order of one second or less, one can achieve significant cost reductions by choosing a long storage tube to function as a high-pressure reservoir in the following way: If a valve at the tube end opens the flow path into a Laval nozzle, an almost constant flow rate results, as long as the resulting expansion wave has not returned from its way through the storage tube. This flow phenomenon is used to avoid costly control mechanisms for the flow total pressure and the total temperature, during the tunnel run. The principle of using a blow-down storage tube can be combined with a vacuum tank at the low pressure tunnel end, in order to increase the possible range of test section pressures. The general layout is displayed in Fig. 1. This invention was the basis for the well-known Göttingen Ludwieg tube facility, RWG, that employs three different storage tubes and six different nozzles in order to cover a large Mach number range, from 4 to 12 [2]. This facility has a run time of 0.3 s.
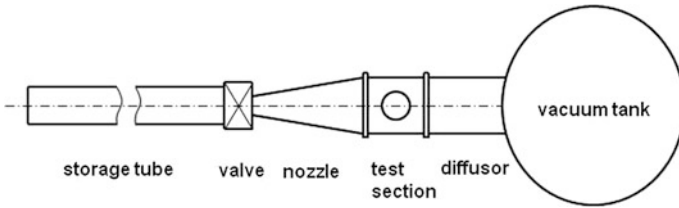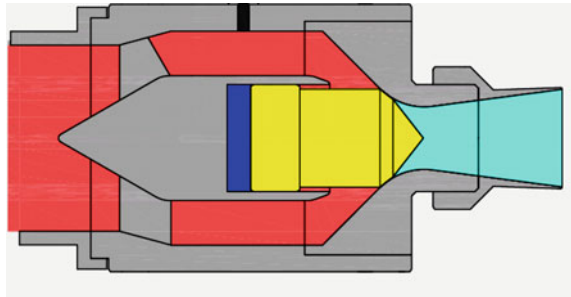
Fig. 1 Working principle of a hypersonic Ludwieg tube

Fig. 2 Schematic drawing of the fast acting valve in closed end position

Over the years progress in flow measurement instrumentation further reduced the run-time requirement. Furthermore, it was recognized that the valve design ahead of the nozzle was critical for further reducing the facility cost. Georg Koppenwallner introduced a new fast acting valve, which was now centered within the flow path towards the nozzle [3]. Here a central piston is pneumatically operated by controlling its back pressure and this feature results in opening times of about 10 ms (Fig. 2).

The gas expansion in the hypersonic nozzle significantly reduces its static temperature. That causes the gas to fall below its saturation curve, if not heated previously. One option is to heat only the part of the storage tube that contains the air which is pushed out during one run. Hence, the storage tube length for a given tunnel run time can be kept as short as possible. Note, that the partially heated tube implies a step in the tube temperature which has to be compensated by a step in the tube diameter, in order to avoid disturbances from the step to be reflected upstream when the expansion wave passes. A reasonable compensation is achieved if the Mach number of the flow behind the expansion wave does not change across the location where the tube temperature changes. Hence, the product of tube area A and speed of sound, i.e. the temperature T, must be constant [3]:

$$A_1\sqrt{T_1} = A_2\sqrt{T_2}$$

For given diameters of storage tube and test section there exist two options to change the test section Mach number:

– Variation of the Laval nozzle throat diameter: Changing the throat changes the nozzle mass flow and hence the storage tube Mach number through the tunnel. Increasing this Mach number above its typical design value as discussed below results in a continuous pressure drop during the run time, because of increase in the wall boundary layer along the storage tube walls, which is undesirable. Hence, the test section Mach number can be merely increased by inserting smaller throats or even complete nozzles.
– Use of a tandem nozzle: Here the original Laval nozzle is replaced by a steep nozzle and a settling chamber, which serve together as a throttling device. This reduces the specific mass flow that now fills the throat of the second nozzle, to yield the desired lower Mach number in the test section [3].

Based on these preliminary considerations the overall layout of a Ludwieg tube begins with defining the design Mach number in the test section. Choosing a low value has several advantages: (1) As flow density drops rapidly with Mach number the unit Reynolds number for a given storage tube pressure also drops with rising Mach number. (2) Lower Mach numbers require lower storage tube temperatures, in order to avoid condensation effects in the test section. This creates less severe problems with natural convection in the storage tube, and entropy fluctuations in the test section flow will be smaller. (3) Lower storage tube temperatures allow using oil particles for seeding the wind tunnel flow. This is important for application of Particle Image Velocimetry. As a consequence the test section Mach number is chosen as low as possible to achieve typical hypersonic flow behaviors in inviscid gas dynamics and boundary layer flows. The general belief is that these behaviors are reasonably well obtained with a test section Mach number of 6.

The test section size is determined by technical and operational reasoning. While a given Reynolds number depends linearly on the storage tube pressure and the model size, practical model manufacture and instrumentation considerations call for choosing the test section as large as possible. For example, measurements of boundary layers in transition research make it very difficult to resolve the higher frequencies and smaller spatial scales of flow instabilities observed on smaller models, at the same Reynolds number. Also, it can be shown that the relative disturbance level due to nozzle boundary layer noise is larger for smaller nozzles [4]. Hence, smaller test sections generally exhibit a larger unit Reynolds number effect on boundary layer transition. Moreover, significant benefits result from the possibility to share wind tunnel models between existing wind tunnels. As many existing hypersonic wind tunnels of leading research establishments have a test section diameter of around 500 mm, this size is advantageous in this respect. It can be concluded that a test section diameter of 500 mm represents an excellent choice for a facility dedicated to fundamental flow research.

An important choice concerns the placement of the tunnel valve. Locating the valve just at the end of the storage tube, as in Fig. 1, will usually create significant disturbances of the flow that enters the nozzle. The result will be a turbulent nozzle

boundary layer and hence noise levels observed in the test section will be at conventional, noisy levels. An alternative is to place the valve behind the test section. Hence, the entrance to the wind tunnel nozzle can be shaped in a completely smooth way, thereby allowing for laminar boundary layers [5]. A low-cost mechanical solution is to place a diaphragm within the tunnel diffuser. However, this location has two disadvantages: (1) Wind tunnel nozzle and test section are now part of the high-pressure wind tunnel components and need a corresponding construction and safety rating. Similarly, the wind tunnel models experience much higher mechanical loads during the tunnel start-up process. (2) The start-up process of the steady tunnel flow is much more affected by model blockage. This limits the possible model size and the Reynolds number. As a thumb rule, the allowed model size of a blunt geometry is twice as large for a tunnel valve located upstream of the nozzle, compared with the downstream position.

Next, the storage tube diameter needs to be determined. As the tunnel throat diameter is given by the test section Mach number and its diameter, the storage tube diameter directly determines the storage tube Mach number. A low storage tube Mach number generally leads to better flow uniformity in the test section. Moreover, due to the growing boundary layer in the storage tube, static pressure slightly drops during tunnel run and this effect becomes larger for increasing storage tube Mach number. It turns out that this effect is rather small for storage tube Mach numbers of around 0.05 while an undesired pressure drop would result at significant larger values [3, 6]. Finally, the desired test time determines the storage tube length. For low values of the storage tube Mach number the test time is approximately determined by

$$t = \frac{2 L_1}{a_1} + \frac{2 L_2}{a_2}.$$

Here the two terms take into account, that the storage tube may be composed of two parts with different lengths, L, and with two different temperatures and correspondingly different sound speeds, a. A suited test time is assumed to be 100 ms.

3 Tunnel Components

These considerations of hypersonic wind tunnel layout lead to the actual design of the Hypersonic Ludwieg Tube Braunschweig (HLB) [7]. The overall design drawing is displayed in Fig. 3.
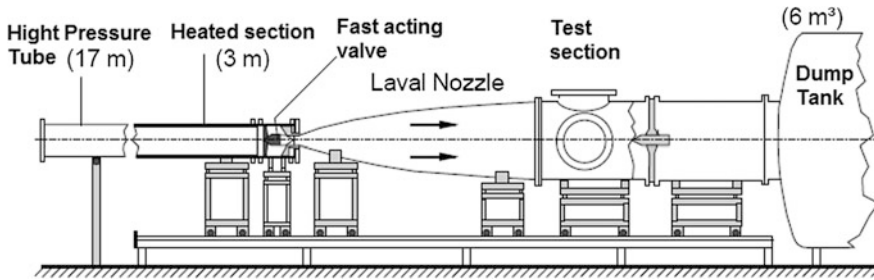
Fig. 3 Overall design drawing of the hypersonic Ludwieg tube Braunschweig

3.1 Storage Tube and Valve

The high pressure section consisting of a 17 m long storage tube with a 3 m long heated section and a valve housing that can be pressurized up to 30 bar. The chosen Mach number of the storage tube placed upstream of the nozzle throat, $M_1 = 0.059$ determines the throat area ratio, $A^*/A_1 = 0.101$. The static temperature T_1 of the flow behind the expansion wave depends on the stagnation temperature T_0 upstream of the wave and the adiabatic coefficient κ as,

$$\frac{T_0}{T_1} = \left(1 + \frac{\kappa - 1}{2}M_1\right)^2$$

Our experience gained by systematic variations of the storage tube temperature shows that heating the tube up to a temperature around 450 K is sufficient to avoid condensation in the test section. As mentioned above, natural convection causes significant stratification of the heated air in the storage tube, if the cold part is not isolated from the heated part. To avoid this unwanted convection an isolated shutter is installed at the end of the heated section [8]. It is opened only shortly before a run. The cross-sectional area blocked by the opened shutter is smaller than the area difference between heated and non-heated section. Therefore the shutter should not impose any additional disturbances on the passing expansion wave. With this shutter the temperature difference due to stratification is reduced to about 20 K. It should be noted that future constructions of similar Ludwieg tubes should employ a longer, completely heated and fully isolated storage tube, to avoid stratification in the storage tube as much as possible.

The fast opening valve used to control the wind tunnel run is sketched in Fig. 2. The valve housing also holds the flow probes used to define the flow state in the tunnel. These are a static pressure gauge and thermocouples located at three circumferential positions in the annular clearance around the valve. The thermocouples have a rise time of about 4 ms. The data from these probes is also used for monitoring homogeneity of the tunnel static temperature during the tunnel run.

3.2   Nozzle

The low pressure section of the HLB consists of the nozzle, the test section, the diffusor and the 6 m³ dump tank. The geometrical definition of the hypersonic nozzle is seen in Fig. 4.

It is comprised of a convergent, conical entry, a subsonic circular contour towards the throat, a transition section to the divergent conical section with an opening angle θ_B, and a polynomial that determines the flow straightening to the final divergence angle θ_A. These geometry parameters were determined by using results of numerical flow simulations as a guideline [9], see Fig. 5.

These simulations assumed fully turbulent boundary layer flow. The analysis of a reference configuration that employed a short transition section with a constant radius of curvature and a simplified polynomial for the flow straightener revealed two sources of compression waves in the nozzle: (1) the overexpansion of the flow in the transition section behind the throat and (2) the curvature distribution in the flow straightener section. These compression waves are observed in the nozzle flow field as depicted in Fig. 5. Note that in all further design calculations the final
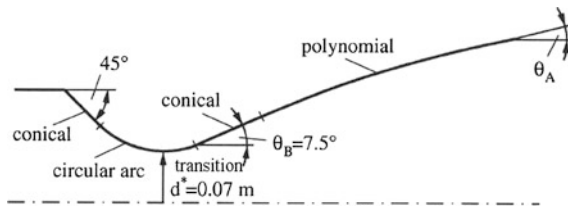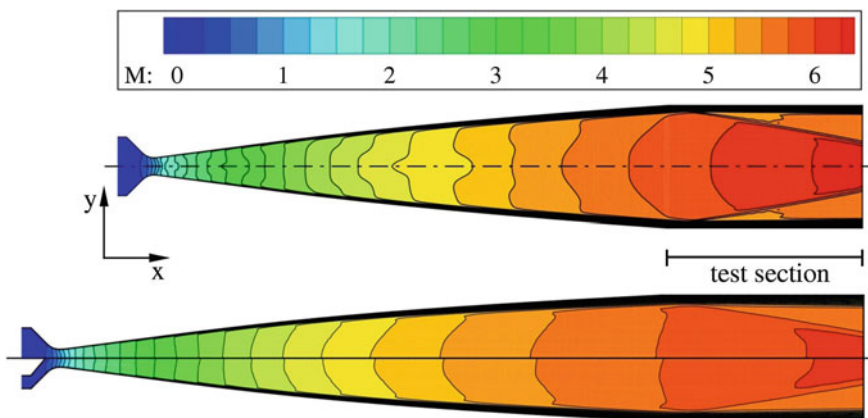

Fig. 4 Nozzle geometry

Fig. 5 Mach number contours of the reference nozzle (*top*) and the optimized nozzle (*bottom*), where the effect of simulating the valve geometry is also displayed [9]

divergence angle, θ_A, was fixed at a value of 3°. This value was chosen based on previous observations, that hypersonic nozzles are sensitive to small changes in flow conditions, and that a fully expanded nozzle would represent an unnecessary risk. The compression wave caused by overexpansion of the supersonic flow into the divergent nozzle section was successfully diminished by using a suitable super-ellipse segment instead of the circular arc. This allowed control of the curvature distribution. The compression wave created by a discontinuous curvature in the initial polynomial of the flow straightener can be avoided as well, by using an improved polynomial with a continuous curvature distribution along the nozzle axis. This yielded a rather smooth flow in the final nozzle geometry. Also seen in Fig. 5 is the influence of the centrally mounted valve on the supersonic nozzle flow. Due to losses in the valve boundary layer, the flow near the axis exhibits a wake-type velocity distribution. This local effect is very limited, i.e. the related deviations in test section Mach number are in the order of 0.02.

3.3   Test Section and Diffusor

The test section has a diameter of 496 mm and a length of 940 mm. Optical access is provided by using three windows with diameters of 265 mm. Two of the windows are located at the test section lateral sides, and these are needed for schlieren optics. The third window allows a view into the test section from above. This is often used for infrared thermography. The cylindrical diffuser section is located downstream of the test section. Its purpose is to increase the static pressure downstream of the test section, so that the continuously rising pressure in the dump tank does not lead to early flow break down. Pressure recovery in the diffusor is usually provided by the wind tunnel model, as the compression waves of the model are repeatedly reflected in the diffuser section.

4   Instrumentation

4.1   Pressure Measurements

The mean flow in the test section is probed by using a rake of 6 Pitot tubes that can be electrically traversed in x- and z-directions as shown in Fig. 6. The xz-traverse is mounted in housing just below the test section. SCC15A pressure transducers of Co. Sensortechnics yield a temporal resolution of around 1 kHz for the Pitot pressures. These sensors measure total pressures. Zero point calibration of the sensors can easily be accomplished, since the test section is evacuated before every tunnel run to around 2 mbar. The temperature effect on the sensor reading was also determined.

High-resolution pressure fluctuation measurements are performed with M131A31 sensors (Co. PCB Piezotronics, Inc.). In the past years, these sensors are

Fig. 6 Drawing of test section with Pitot rake and xz-traverse, from [7]
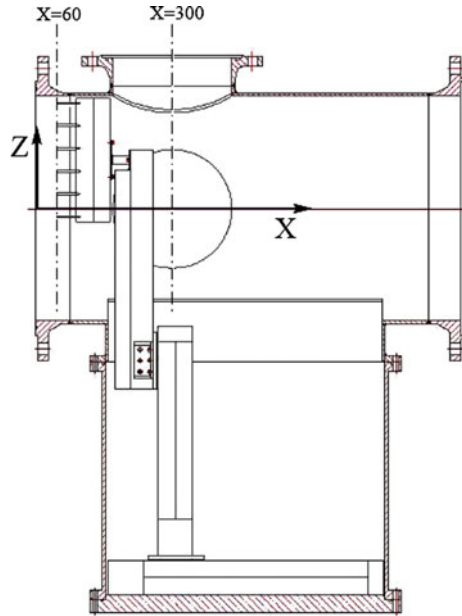
widely used for measurements of hypersonic boundary layer instabilities (see, e.g., among many others, Estorf et al. [10] or Heitmann et al. [11]). According to the manufacturer's specification the resonance frequency of the sensor is larger than 1 MHz and the output signal is high-pass filtered at 10 kHz. The nominal diameter of the active sensor face is 3.18 mm, however, it is known that the active sensor area is much smaller, i.e. 0.76×0.76 mm^2 [12]. Hence the sensor can resolve very small flow structures. Power is supplied by two PCB instruments (M482A22 and M483A), which, at the same time, perform signal conditioning. The sensors have sensitivities in the range of 0.02 mV/Pa and a nominal resolution of 7 Pa. The pressure data is sampled with a Spectrum M2i.4652 transient recorder, having a sampling frequency of 3 MHz. Time traces of 265 ms length are usually recorded, consisting of about 180 ms before/after and 80 ms of data during the tunnel run.

4.2   Schlieren

The schlieren set up used in the HLB is sketched in Fig. 7. A virtual image of the light source Q is generated at the knife edge (a disc with a central hole) K, so that only part of the light beam can pass through. The part of the beam that passed through K is focused at the spherical mirror S that has a curvature radius of 6 m. As mentioned the schlieren knife-edge, K provides selective shading of the light passing through the test section. It is redirected towards the camera by beam splitter T.
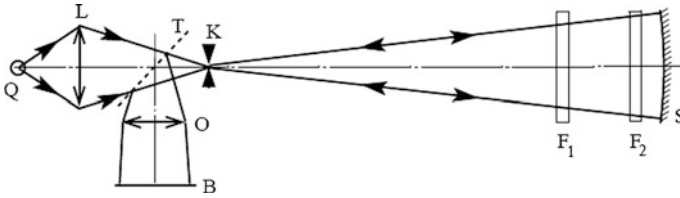
Fig. 7 Layout of HLB schlieren optics: *Q* light source, *L* lense, *K* knife edge, schlieren edge, *F* test section windows, *S* spherical mirror, *T* beam diverter, *O* camera lense, *B* schlieren image

4.3 Heat Flux

For optical measurements of wind tunnel model temperatures an infrared camera, Phoenix DAS of the Indigo Company is available. The camera uses a Stirling-cooled InSb-sensor which is sensitive in the middle infrared range, between 3 and 5 μm. The camera allows recording images with 320×256 pixels at frame rates up to 320 Hz. Typical integration time at temperature of 300 K are 3 ms, in order to achieve a good signal-to-noise ratio. This results in frame rates of 170 Hz. Optical access of the camera to the test section is obtained by using a sapphire window.

For temperature calibrations a black radiator is installed in place of the model before measurements. The temperature calibration curve is computed using a quadratic fit of the calibration points. The non-uniformity of the pixel-sensitivities is eliminated by a two-point correction, assuming that the pixel sensitivities differ only in the linear terms.

Wind tunnel models suited for infrared measurements are made from Plexiglas (black 811-Rhm-GS) and coated with Nextel Velvet Coating 811-21 at thickness of approximately 50 μm. This choice is the result of extensive studies in model materials [13], where the surface emissivity and material absorption were carefully measured. Note that the effects of temperature dependent thermophysical properties of the model material were also investigated [14, 15].

Image coordinates are mapped to space coordinates by using a calibration grid which is applied to the surface of the model before measurements. The currently implemented calibration software detects the image coordinates of the grid nodes and determines numerical functions for mapping curved surface coordinates into a Cartesian system [13]. This spatial calibration method is well suited for the images of axisymmetric model geometries.

1D nonlinear heat conduction perpendicular to the surface is assumed for calculating the surface heat fluxes from the transient temperature data. For this purpose the conduction into the Plexiglas is modeled by a finite difference method. The unknown heat flux is found by iterative regularization method: The surface temperature calculated from an iteratively improved heat flux is compared with the measured value in a least squares formulation. The gradient for iterative correction of the heat flux is found by solving the adjoin problem. Iteration end is adjusted to

the noise level of the measured temperature data. Details of heat flux calculation with an extensive discussion of measurement errors can be found in [13]. There the overall uncertainty of the measured heat flux is estimated to be about 4 %.

High-frequency time resolved heat flux measurements are performed with a fast response heat flux sensor (ALTP, Atomic Layer Thermopile) [16]. The measuring method is based on the transverse Seebeck effect which allows measuring directly the heat flux density. The sensitive area has a size of 2 mm × 1 mm. As the ALTP sensors are powered with a low-noise amplifier from Cosytech, the output signals are amplified with an adjustable gain from 100 to 800 for the DC output and fixed amplified with a rate of 5000 for the AC output. The thermal insulation of the gauge is achieved via a ceramic housing and has a diameter of 8 mm.

5 Wind Tunnel Flow

5.1 Flow Start

The low pressure section of the HLB comprising of the nozzle, the test section, the diffuser and the 6 m^3 dump tank are evacuated to about 3 mbar before a tunnel run. The storage tube is pressurized up to 30 bar. Figure 8 displays an example of the measured transient distributions of static pressure recorded by the sensor in the annular duct around the valve and the test section Pitot pressure, upon the valve opening. After the initial transient, virtually constant pressures are observed. After 90 ms run time, pressures drop due to the travelling expansion wave in the storage tube that reaches the nozzle. The rising pressure in the dump tank causes break down of the test section flow at 110 ms, which is seen in the sudden rise in the recorded Pitot pressure. Shortly thereafter, the valve closes. The oscillations of the storage tube pressure at the beginning of the tunnel run could be traced back to the first mode of transversal oscillations in the tube, according to their frequency [15]. A measurable effect of these oscillations in the test section has not been observed.

Fig. 8 Example of recorded pressure distribution in the storage tube and in the test section
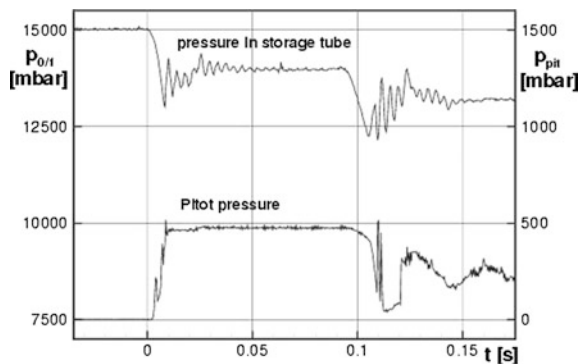
The initial transient of the tunnel flow initiation was further investigated by using time-accurate, numerical flow simulations [15]. Because of limited computational resources, the assumption of axially symmetric flow within the storage tube, valve and nozzle was invoked. Numerical resolution of shock waves and contact discontinuities was accomplished by employing a hybrid flux vector scheme, AUSMPW+, for discretizing the inviscid fluxes. Turbulent wall boundary layers were modeled by employing the Menter-SST eddy viscosity model. The computations with the DLR TAU flow solver [17] used a deforming mesh in order to account for the piston motion during the valve opening. Therefore, the piston motion was measured as shown in Fig. 9. The piston velocity exhibits an oscillatory behavior during the opening phase which results from the dynamics of the pneumatic system involved.

The numerical results are used for understanding the complex flow physics during the valve opening and the initial transient flow into the test section. Figure 10 displays computed density gradients at several time instances. The initial flow shortly after the piston motion started displays the primary shock and the
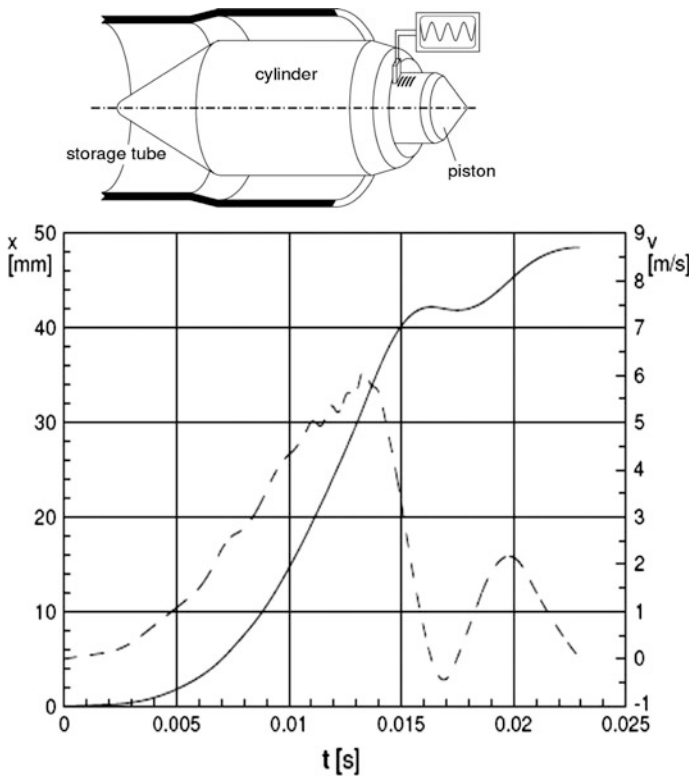

Fig. 9 Measured piston position and velocity during the valve opening. With kind permission from Springer Science+Business Media: [15], Fig. 2

contact discontinuity which run into the nozzle. Later, the initial expansion wave that propagates into the storage tube is seen. The initial flow structure in the nozzle is characterized by a very small annular throat between the piston and the converging nozzle contour. This configuration leads to strong expansion-flow rates and a number of shocks, which generate significant flow separation in the divergent part of the nozzle.

As the piston moves backwards, the increasing annular throat delivers a larger mass flow into the nozzle and the flow separation disappears (t = 5 ms). At this point the critical flow state is still located between the piston and the converging nozzle contour and hence, a strong oblique shock wave is generated with multiple reflections along the nozzle. This situation changes when the critical flow state moves to the geometrical nozzle throat at about 9.25 ms. From this time on a rather smooth nozzle flow develops which is increasingly less distorted by the piston.
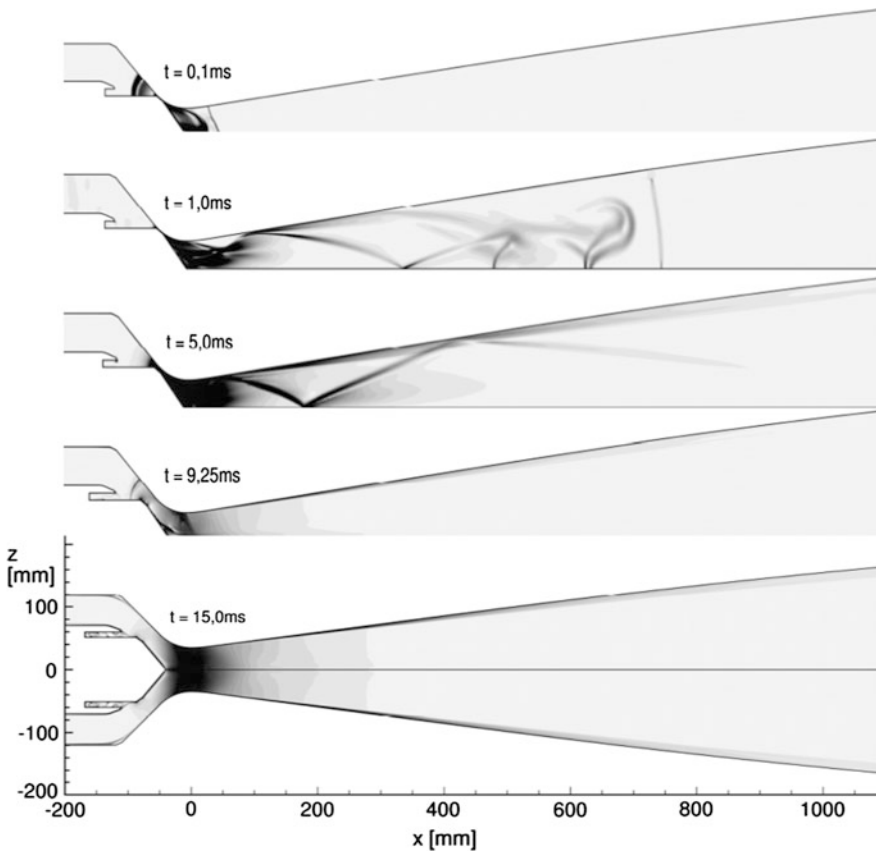

Fig. 10 Temporal flow development in HLB nozzle [17]. Shown are density gradient contours for an initial storage tube pressure of 3.25 bar. The initial pressure in the nozzle is 2 mbar. With kind permission from Springer Science+Business Media: [15], Fig. 7

Fig. 11 Time history of
computed Mach number at
test section entrance for two
storage tube pressures. With
kind permission from
Springer Science+Business
Media: [15], Fig. 9
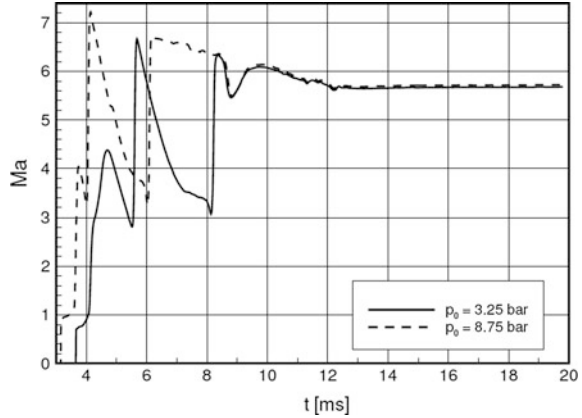
Further details regarding the computed flow development are available in [15] and
in [17], where also the flow entering the test section is characterized. Figure 11
displays the Mach number at the test section entrance as an example. It is seen that
details of the flow development depend on the initial storage tube pressure.
Nevertheless, the flow state appears virtually constant after 14 ms.

5.2 Test Section Flow

The test section flow is characterized by using measured data of the mean flow and
its fluctuations. The Pitot rake shown in Fig. 6 was used for determining the Mach
number in the test section. The flow field was traversed at a number of x-positions.
The mean values of the Pitot pressure were obtained by averaging the data between
35 ms and 80 ms after starting the flow in the tunnel. The results for a representative
storage tube pressure of $p_0 = 15$ bar are shown in Fig. 12. The measurement
accuracy corresponds roughly to the symbol size in Fig. 12. The full line is the
numerical result obtained for a steady-state flow computation, which appears to be
in good agreement with the measured distribution. The measured data exhibit a
compressive Mach wave which focuses at the tunnel centre. The Pitot readings
exhibit local peaks where the wave passes, which is obviously due to the interaction
of the wave with the Pitot-tube bow shock. The most probable origins of this wave
are junctions between different nozzle segments downstream of the nozzle throat.

The Mach number of the HLB test section is then defined at the reference
position, $x = 300$ mm, $z = 100$ mm, based on the measured Pitot data and the
corresponding numerical simulations [13]. It varies slightly with the Reynolds
number:

Fig. 12 Distribution of Pitot
pressures in the test section
for $p_0 = 15$ bar
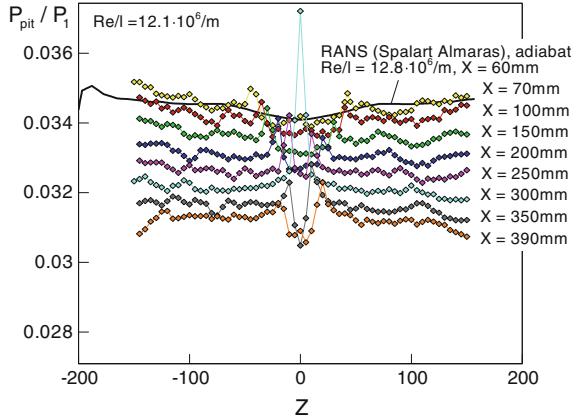
$$M_\infty = \begin{array}{ll} 5.91 \pm 0.03 & for \quad p_0 = 15.0\,\text{bar} \\ 5.85 \pm 0.03 & for \quad p_0 = 3.25\,\text{bar} \end{array}$$

The assumption of isentropic nozzle flow and the reference Mach number are used for determining the reference free-stream pressure:

$$p_\infty = (0.9327 \pm 0.0007)\left(1 + \frac{\gamma - 1}{2}M_\infty^2\right)^{\frac{\gamma}{1-\gamma}} p_0,$$

where p_0 is the storage tube pressure measured before flow initiation. Readings of the thermocouples in the annual clearance around the valve are used for obtaining the total temperature of the tunnel flow. Further measurements of test section temperatures available in [18] indicate that the measured total temperature is a reasonable representation for the reference test section position with an uncertainty of ± 5 K. Hence

$$T_\infty = \left(1 + \frac{\gamma - 1}{2}M_\infty^2\right)^{-1} T_{1t} = (0.1256 \pm 0.0011)T_{1t} \pm 0.6\ \text{K}$$

where T_{1t} denotes the storage tube total temperature as measured at the valve housing. The Reynolds number per unit length in the test section can be computed from these values and by assuming a suitable viscosity law [13]. Similarly, a reference heat flux density is computed in order to determine the non-dimensional Stanton numbers from measured heat fluxes. The given uncertainties for freestream Mach number, pressure, and temperature can be combined to obtain uncertainties for the reference values of the Reynolds number and the heat flux as detailed in [13].

Pressure and heat flux fluctuations were determined by using stagnation probes. Figure 13 shows amplitude spectra of normalized Pitot pressure fluctuations, at a
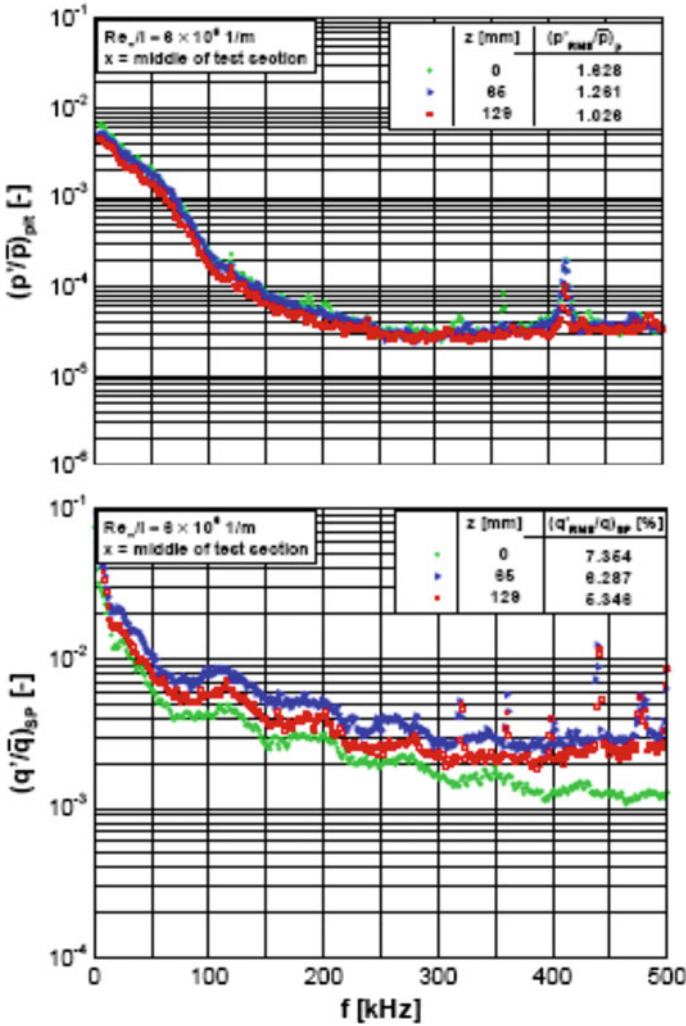
Fig. 13 Spectra of normalized Pitot pressure fluctuations (*left*) and normalized heat flux fluctuations (*right*) at a unit Reynolds number of 6×10^6/m and $T_{1t} = 480$ K [19]

unit Reynolds number of 6.0×10^6/m at three positions in the vertical symmetry plane of the test section. All three spectra show a noticeable peak at about 410 kHz, representing the natural frequency of the used Entran EPIH-113-1B/Z1 sensor. A typical decay of the fluctuation level versus frequency without considerable dominant peaks is visible in this figure. The rms-values of the normalized Pitot pressure fluctuations are between 1–1.6 % and increase towards the centerline. Figure 13 also shows the amplitude spectrum of the heat flux fluctuation in the stagnation point of the blunt body normalized by the corresponding mean heat flux

density obtained simultaneously. The rms-values of the normalized fluctuations are between 5.3–7.3 % and increase towards the centerline, like the pressure fluctuations.

5.3 Reference Model Testing

Testing of two reference model geometries yields further insight into the quality of the used instrumentations and the behavior of the test section flow. The first model geometry is chosen for evaluating the infrared based heat transfer measurements. The geometry is displayed in Fig. 14. It is an axially-symmetric representation of the HERMES re-entry vehicle with deflected control flap [20]. One wind tunnel model was manufactured from black Plexiglas (PMMA) and painted with Nextel Velvet Coating 811-21. An alternate wind tunnel model was provided by the DLR in Göttingen. This is a thin-wall model which consists of a 0.35 mm nickel layer, to which Nichrome wires are soldered to provide thermocouple contact [21]. The measured temperature change with time is proportional to the heat flux, as detailed in [13]. The flow over the model develops a thin, laminar boundary layer along the
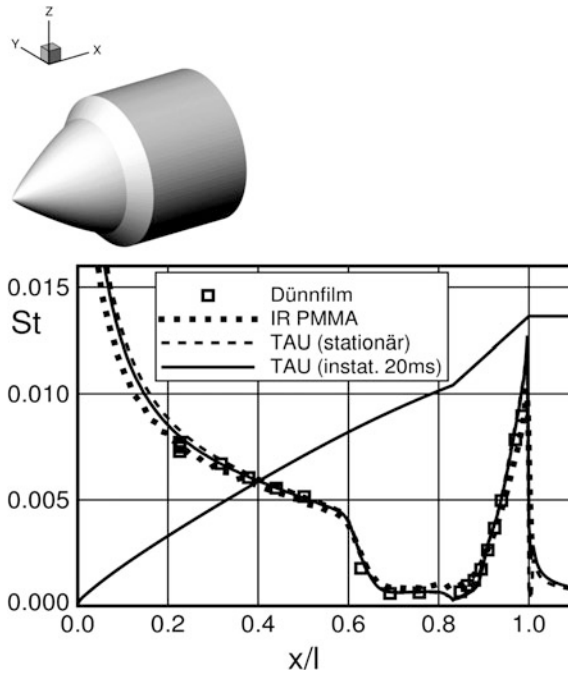

Fig. 14 Stanton number distributions for laminar flow over the hyperboloid and flare configuration, $M_\infty = 5.85$, $p_0 = 3.25$ bar, $T_{1t} = 485$ K, taken from [17]

forebody. The interaction of the boundary layer and the oblique flare shock wave leads to a separation bubble with locally low heat transfer. This is followed by flow re-attachment with a strong overheating. The infrared-based heating result was obtained by inverse solution of the one-dimensional unsteady heat conduction equation at a tunnel run time of 75 ms. The resulting heat flux values were averaged over a model segment of 20° in circumferential direction. Figure 14 displays very good agreement between the two measurements and the two corresponding numerical flow simulations. One of these flow simulations, with the DLR-TAU Code, used the unsteady start-up of the test section flow shown in Fig. 10 as a non-stationary onset flow. The other numerical simulation used the flow conditions at the test section reference point as described above, and assumed a parallel free stream flow. Both simulations resulted in very similar results for the Stanton number, which are in line with the two experimental realizations.

This good agreement confirms the experimental approach of defining suited reference flow conditions for the HLB test section flow. Further analysis of uncertainties for the infrared measurements is available in [13], it revealed that the remaining uncertainties due to coating transparency and due to errors of the wind tunnel reference heat flux are similarly large. Both errors yield uncertainties in the Stanton number of 3–4 % of the measured value.

The level of the free stream disturbances in HLB is indirectly assessed by investigating laminar boundary layer instabilities and boundary layer transition on a pointed circular cone. Using a 7° half-angle cone model equipped with a stream-wise array of PCB M131A31 sensors, pressure fluctuations due to second-mode instability were measured for different storage tube pressures and hence, different Reynolds numbers. Similarly, the point of a complete transition laminar-turbulence was identified by measuring the location of maximum heat flux along the cone using infrared thermography. The results are displayed in Fig. 15 along with the transition correlation of Pate [4].

Fig. 15 Distributions of pressure fluctuations and heat flux along the 7° cone in HLB, T_{t1} = 480 K taken from [22]
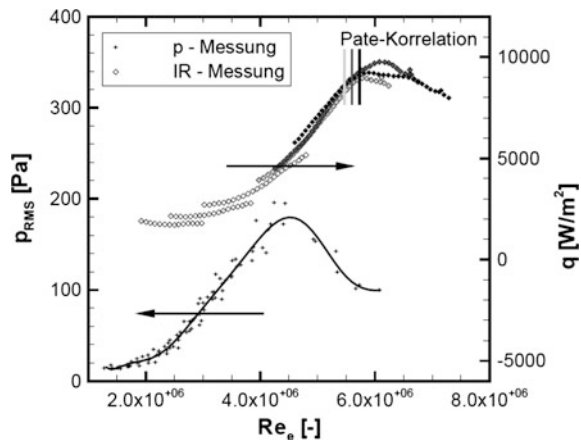
Here, computed flow quantities at the boundary layer edge of the cone flow are used to plot the measured boundary layer data. The Pate correlation estimates the effect of wind tunnel noise from the turbulent nozzle boundary layer on hypersonic transition for cones. It is seen that transition in HLB appears somewhat downstream of the Pate correlation, presumably because fluctuations in Ludwieg tubes are relatively low compared to other blow-down facilities. However, the expected effect of unit Reynolds number is represented in the HLB test section.

6 Experiments in Transitional Hypersonic Boundary Layers

Recent boundary layer research in the Hypersonic Ludwieg Tube Braunschweig aims at identifying and characterizing the instabilities of the laminar boundary layer that lead to laminar-turbulent transition. So far the work focused on harmonic modes with exponential growth. Progress in the development of suited wind tunnel models and model instrumentation has resulted in the ability to determine the frequency and amplification of harmonic modes in the boundary layer, the orientation of wave fronts and the size of typical wave packets.

The experimental work used the circular 7° sharp cone as a generic model of slender hypersonic vehicles. Several wind tunnel models were manufactured of coated Plexiglas and instrumented with PCB M131A31 sensors. These sensors exhibit a very high sensitivity and their temporal resolution is sufficient for resolving high-frequency modes observed in hypersonic boundary layers [10]. Infrared analysis of the surface temperature allows monitoring the flow break down to turbulence and can be used to detect stationary instability modes as well.

A recent experimental approach assumes that instabilities may be characterized by using space-time cross correlations. Variation of the spatial distance in these correlations can be accomplished with sensors placed on rotatable discs. Figure 16 displays such a wind tunnel model.

For model accuracy, the discs are mounted on a single model axis with high precision bushings. 10 PCB sensors are installed on three rotatable discs with their sensing head mounted flush to the surface. The first disc has a stainless steel tip and carries sensors 0, 1, 2 used to measure initial growth of the boundary layer instabilities. Sensors 3, 4, 8 can be rotated, relative to sensor 2. They are installed closely behind sensor 2. This arrangement is used for measuring space-time correlations.
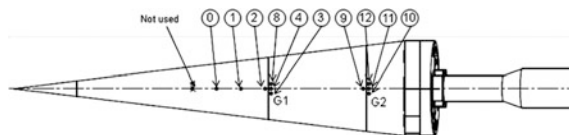

Fig. 16 Sharp cone model with three rotatable discs

A similar group is formed by sensors 9, 10, 11, 12. With these two groups the unit Reynolds number can be varied during experiments. The final model disc accomplishes the model attachment to the model support sting, at the predefined angle of attack.

The dominating instability of streamwise hypersonic boundary layer flow is an acoustic instability. It is called 2nd mode, according to Mack [23]. The amplification rate of the mode in hypersonic flow is much larger than the Tollmien-Schlichting instability (1st mode). Signals from sensors mounted on the cone, installed at zero angle of attack show that the 2nd modes appear as wave packages that grow while travelling downstream. First modes are not detected by the PCB sensors. Figure 17 displays measured data of the 2nd mode behavior. The spectral analysis of the measured fluctuations is also presented. It shows the growth of the modes. Note that the initial growth rates are in good agreement with the result of linear stability analysis (not shown here) [10, 22].

The temporal distributions of two sensor readings can be correlated in order to extract more structural data of the wave packages. Using the measured phase velocity one can interpret the temporal correlation signal as the spatial distribution of wave fronts in a statistically averaged wave package. This is illustrated in Fig. 18 which shows the wave fronts measured at two unit Reynolds numbers. The wave fronts are normal to the streamwise direction, as expected. The measured wave length is close to two boundary layer thicknesses. The lateral extension of the average wave package is 4–5 boundary layer thicknesses.

The flow over the sharp cone at angles of attack develops a more complex set of boundary layer instabilities. These are streamwise 2nd modes as well as instabilities due to the boundary-layer cross flow. The observed infrared-based surface heat flux shown in Fig. 19 underlines the complexity of the 3-dimensional boundary layer flow. Plotted are colored heating contours as a function of the cone x-coordinate and the cone azimuthal angle, θ. The value $\theta = 0°$ denotes the windward side of the cone, whereas $\theta = 180°$ is at the leeside. The break down to turbulence is indicated by the rapid color change from green to red.

At the windward side the transition front displays a smooth behavior and only 2nd mode instabilities have been measured in this area so far. At the cone shoulder a zigzag behavior of the transition front is observed and longitudinal flow structures appear in the heat flux distribution. This is typical for transition dominated by stationary cross flow vortices. However, the signals from the PCB sensors at locations between 70° and 110° reveal that other instabilities are also present. Figure 20 presents a spectrum obtained with the sensors located at $\theta = 70°$.

One observes the 2nd mode at a high frequency of 350 kHz. Moreover, there is a distinct peak in the signal of the sensor group 2, at 30 kHz. The time traces were then similarly analyzed by evaluating cross correlations. These revealed rather large wave packages with an oblique wave structure as seen in Fig. 21. The wave front
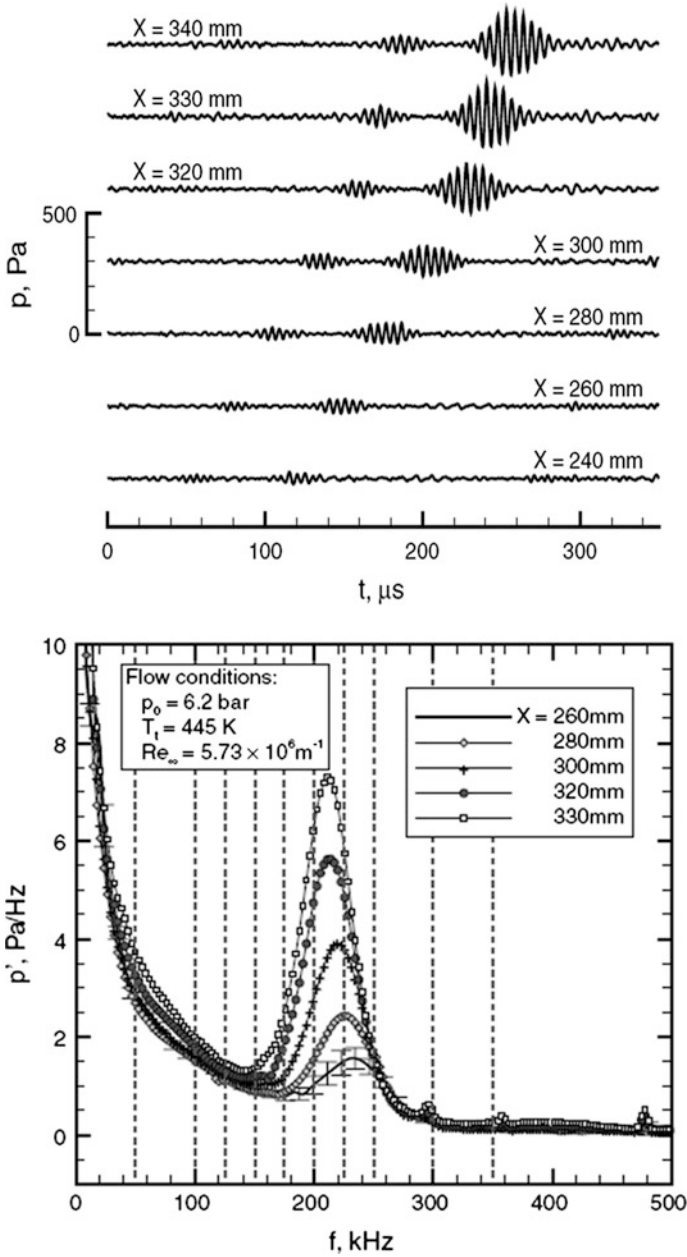
Fig. 17 Time traces and disturbance spectra from PCB M131A31 sensors on a 7° cone, Re/m = 5.7 × 10^6/m. From [24]; reprinted by permission of the American Institute of Aeronautics and Astronautics, Inc.
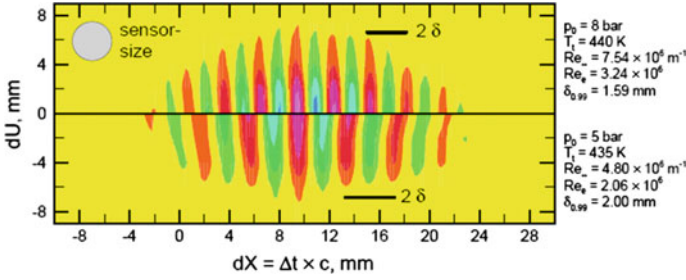
Fig. 18 Contours of measured cross correlation between PCB sensor signals, displaying averaged wave packages of 2nd instability modes. From [24]; reprinted by permission of the American Institute of Aeronautics and Astronautics, Inc.
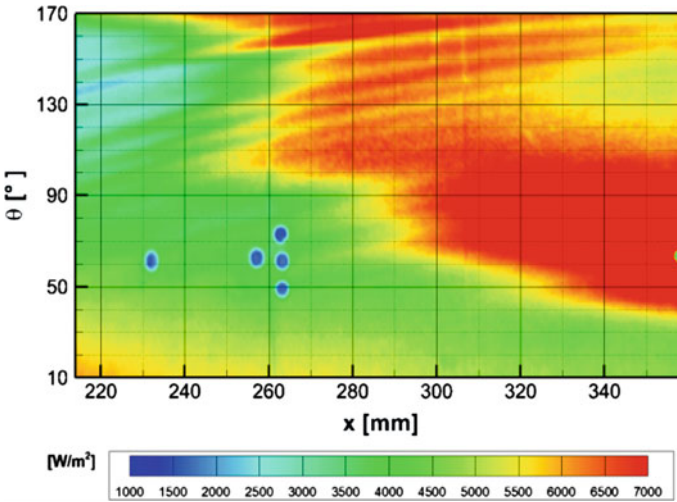

Fig. 19 Heat flux contours of inclined circular cone, for Ma = 5.9, Re/m = 1.1×10^7 m^{-1}, $\alpha = 6°$, taken from [25]

angle with respect to the boundary layer edge flow direction could be also determined from the correlation data [25]. Comparisons with recent numerical simulations of this flow [26] reveal that we have measured travelling cross-flow modes at the cone shoulder. These experiments were successful in that three different
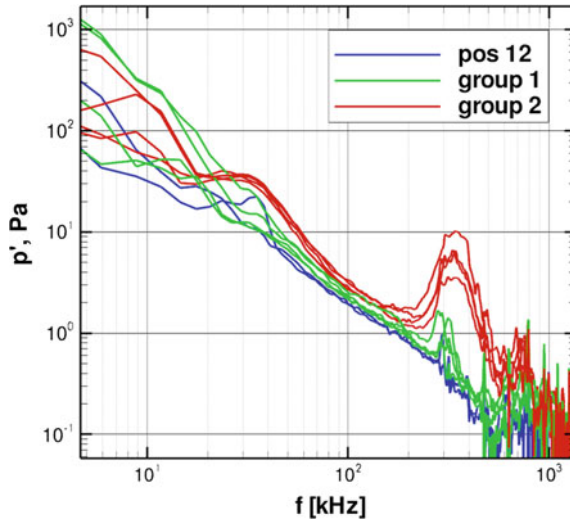
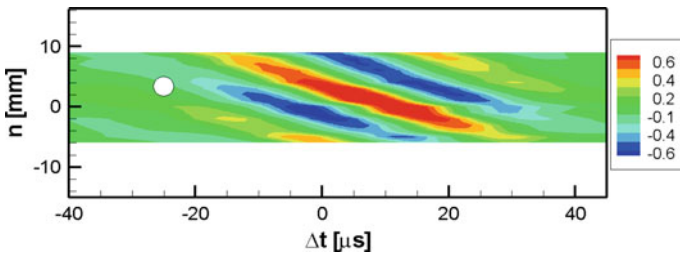**Fig. 20** Spectra of PCB sensors on the circular cone of Fig. 16 at Re/m = 3.64 × 10^6, α = 6° and θ = 70°, taken from [25]

Fig. 21 Space-time correlation from band-pass filtered PCB signals of the circular cone at x = 360 mm and θ = 70° and Re/m = 3.64 × 10^6, α = 6°, taken from [25]

boundary layer instabilities were simultaneously measured for the first time. As the flow is complex, more investigations are planned to understand better the sensitivities of cross flow dominated transition in hypersonic boundary layers.

References

1. Ludwieg, H.: Der Rohrwindkanal. Z. f. Flugwiss. **3**, 206–216 (1055)
2. Ludwieg, H., Hottner, T., Grauer-Carstensen, H.: Der Rohrwindkanal der Aerodynamischen Versuchsanstalt Göttingen, Jahrbuch 1969 der DGLR, 1969, pp. 52–58
3. Koppenwallner, G., Müller-Eigner, R., Friehmelt, H.: HHK Hochschul Hyperschall-Kanal: Ein "Low Cost" Windkanal für Forschung und Ausbildung, DGLR Jahrbuch **2** (1993)

4. Pate, S.R., Schueler, C.J.: Radiated aerodynamic noise effects on boundary-layer transition in supersonic and hypersonic wind tunnels. AIAA J. **7**(3), 450–457 (1969)
5. Schneider, S.P.: Development of hypersonic quiet tunnels. J. Spacecraft Rockets **45**, 641–664 (2008)
6. Koppenwallner, G., Hefer, G.: Kurzzeitversuchsstand zur Treibstrahlsimulation bei hohen Drücken. DFVLR, IB 252-76 H 12, Göttingen, 1976, (unpublished)
7. Estorf, M., Radespiel, R., Heine, M., Müller-Eigner, R.: Der Hyperschallwindkanal Ludwiegrohr Braunschweig HLB. DGLR-Jahrbuch **1**(2003), 661–670 (2003)
8. Estorf, M., Wolf, T., Radespiel, R.: Experimental and numerical investigations on the operation of the hypersonic Ludwig Tube Braunschweig. In: Proceedings 5th European Symposium on Aerothermodynamics for Space Vehicles, pp. 579–586. 8–11 Nov 2004, ESA SP-563, 2005
9. Kozulovic, D., Radespiel, R., Müller-Eigner, R.: aerodynamic design parameters of a hypersonic ludwieg tube nozzle. In: Zeitoun, D.E., Periaux, J., Desideri, J.A., Martin, M. (eds.) Conference Proceedings: West East High Speed Flow Fields, 2002
10. Estorf, M., Radespiel, R., Schneider, S.P., Johnson, H.B., Candler, G.V., Hein, S.: Surface-pressure measurements of second-mode instability in quiet hypersonic flow. AIAA Aerospace Sciences Meeting, AIAA Paper 2008-1153, 2008
11. Heitmann, D., Rödiger, T., Kähler, C. J., Knauss, H., Radespiel, R., and Krämer, E., Disturbance-Level and Transition Measurements in a Conical Boundary Layer at Mach 6, 26th AIAA Aerodynamic Measurement Technology and Ground Testing Conference, AIAA Paper 2008-3951, 2008
12. Rufer, J., Berridge, D.C.: Experimental study of second-mode instabilities on a 7-Degree Cone at Mach 6, AIAA Paper 2011-3877, 2011
13. Estorf, M.: Ortsaufgelöste Bestimmung instationärer Wärmestromdichten in der Aerothermodynamik. ZLR-Forschungsbericht 2008-03, Shaker Verlag, Aachen, 2008
14. Estorf, M.: Ortsaufgelöste Bestimmung instationärer Wärmestromdichten aus thermografischen Messungen, Deutscher Luft- und Raumfahrtkongress 2008, Paper No. 81344, 2008
15. Wolf, T., Estorf, M., Radespiel, R.: Investigations of the starting process in a Ludwieg Tube. Theor. Comput. Fluid Dyn. **21**, 81–98 (2007)
16. Knauss, H., Roediger, T., Gaisbauer, U., Kraemer, E., Bountin, D.A., Smorodsky, B.V., Maslov, A.A., Sruljes, J., Seiler, F.: A novel sensor for fast heat flux measurements, AIAA Paper 2006-3637, 2006
17. Wolf, T.: Strömungsanalyse und Wärmeübergang beim Startvorgang eines ventilgesteuerten Ludwieg-Rohres. ZLR-Forschungsbericht 2007-06, Shaker Verlag, 2007
18. Estorf, M., Wolf, T., Radespiel, R.: Experimental and numerical investigations on the operation of the Hypersonic Ludwig Tube Braunschweig. In: 5th European Symposium on Aerothermodynamics for Space Vehicles, pp. 579–586. ESA SP 563, 2005
19. Heitmann, D., Kähler, C.J., Radespiel, R., Rödiger, T., Knauss, H., Krämer, E.: Disturbance-level and transition measurements in a conical boundary layer at Mach 6, AIAA Paper 2008-3951, 2008
20. Schwane, R.: Description of the testcase: MSTP Workshop 1996 "Reentry Aerothermodynamics and Ground to Flight Extrapolation". Technical Report YPA/1889/RS, ESTEC, Noordwijk, 1996
21. Krogmann, P.: Hyperboloid/flare experiments at Mach 6.8 in RWG, Technischer Bericht DLR-IB 223-94 C 44, Institut für Strömungsmechanik, DLR Göttingen, 1994
22. Heitmann, D.: Transitionsuntersuchungen in hypersonischen Grenzschichten mit laserinduzierten Störungen. CFF Forschungsbericht 2011-09, Shaker Verlag, 2011
23. Mack, L.M.: Linear stability theory and the problem of supersonic boundary-layer transition. AIAA J. **13**, 278–289 (1975)
24. Heitmann, D., Radespiel, R., Knauss, H.: Experimental study of boundary-layer response to laser-generated disturbances at Mach 6. J. Spacecraft Rocket **50**(2), 294–304 (2013)

25. Munoz, F., Heitmann, D., Radespiel, R.: Instability modes in boundary layers of an inclined cone at Mach 6. AIAA-Paper 2012-2823, 2012
26. Perez, E., Reed, H.L., Kuehl, J.J.: Instabilities on a hypersonic yawed straight cone. AIAA Paper 2013-2879, 2013

Author Biographies

Rolf Radespiel is known for his boundary layer research in high-speed flows at Technische Universität Braunschweig, Germany. He has been extensively using the Braunschweig Ludwieg Tube for this research and his research group presented a number of advanced measuring techniques. He received his "Dipl.-Ing." degree in engineering science from Technische Universität Braunschweig and his "Dr.-Ing." degree from the same University. He presently holds the Chair of Fluid Mechanics in Braunschweig. His current research interests include models of transition and turbulence, further high-lift augmentation and drag reduction by means of flow control.

Malte Estorf worked in the aerothermodynamics group at the Institute of Fluid Mechanics in Braunschweig between 2002 and 2008. He put the Braunschweig Ludwieg Tube into operation and established advanced measurement techniques. He received his "Dipl.-Ing." degree in engineering science from Technische Universität Braunschweig and his "Dr.-Ing." degree from the same University. He presently works for the Volkswagen AG.

Dirk Heitmann received his "Dipl.-Ing." degree in engineering science from Technische Universität Braunschweig in 2005 and his "Dr.-Ing." degree from the same University in 2011. His research focused on boundary layer transition in high speed flows. This work was mainly conducted in the Braunschweig Ludwieg tube. His research interests include boundary layer transition, high speed flows and measurement techniques. He presently works at the DLR Braunschweig in the aeroacoustics department.

Federico Muñoz graduated in 2009 from National University of La Plata, Argentina as Aeronautical Engineer. He has since conducted doctoral studies at TU Braunschweig, by characterizing second modes and cross flow instabilities in hypersonic boundary layers.

Torsten Wolf received his „Dipl.-Ing." degree in engineering science and his "Dr.-Ing." from Technische Universität Braunschweig. His thesis covers the numerical rebuilding of the starting process of the Braunschweig Ludwieg Tube. He currently works in the Turbine Aerodynamics department at Rolls-Royce Deutschland as aerodynamics engineer and project lead of research projects.